 doi:10.20944/preprints202005.0426.v1

Terrestrial laser scanning intensity captures diurnal variation in leaf water potential

Junttila, S.[1,2,*], Hölttä, T.[2], Puttonen, E.[3], Katoh, M.[4], Vastaranta, M.[1], Kaartinen, H.[3,5], Holopainen, M.[2] & Hyyppä, H.[6]

[1] School of Forest Sciences, University of Eastern Finland, Joensuu, 80101, Finland

[2] Department of Forest Sciences, University of Helsinki, Helsinki, 00014, Finland

[3] Department of Remote Sensing and Photogrammetry, Finnish Geospatial Research Institute, National Land Survey of Finland (NLS), Masala, 02431, Finland

[4] Institute of Mountain Science, Shinshu University, 8304, Minamiminowa-Village, Kamiina-County, Nagano 399-4598, Japan

[5] Department of Geography and Geology, University of Turku, 20500 Turku, Finland

[6] Department of Built Environment, School of Engineering, Aalto University, 02150 Espoo, Finland

[*] Corresponding author at: Department of Forest Sciences, University of Helsinki, Larokartanonkaari 7, 00014 Helsinki, Finland. E-mail address: samuli.junttila@helsinki.fi (S. Junttila).

Abstract

Drought-induced plant mortality has increased globally during the last decades and is forecasted to influence global vegetation dynamics. Timely information on plant water dynamics is essential for understanding and anticipating drought-induced plant mortality. The most common metric that has been used for decades for measuring water stress is leaf water potential (Ψ_L), which is measured destructively. To obtain information on water dynamics from trees and forested landscapes, remote sensing methods have been developed. However, the spatial and temporal resolution of the existing methods have limited our understanding of water dynamics and diurnal variation of Ψ_L within single trees. Thus, we investigated the capability of terrestrial laser scanning (TLS) intensity in observing diurnal variation in Ψ_L during a 50 hour monitoring period and aimed to improve understanding on how large part of the diurnal variation in Ψ_L can be captured using intensity observations. We found that TLS intensity at 905 nm wavelength was able to explain 78% of the variation in Ψ_L for three trees of two tree species with a root-mean square error of 0.137 MPa. Based on our experiment with three trees, time-series of TLS intensity measurements can be used in detecting changes in Ψ_L, and thus it is worthwhile to expand the investigations to cover a wider range of tree species and forests and further increase our understanding of plant water dynamics at wider spatial and temporal scales.

Keywords: leaf water potential, lidar intensity, terrestrial laser scanning, diurnal variation, leaf water content, drought, tree health, plant water dynamics

Preprints (www.preprints.org) | NOT PEER-REVIEWED | Posted: 26 May 2020 doi:10.20944/preprints202005.0426.v1

1. Introduction

Global warming is altering global hydrological cycles, which results in intensified and prolonged droughts further causing forest mortality (McDowell and Allen, 2015; Trenberth, 2011). In addition to dry areas getting dryer, more intense precipitation events take place due to increased water holding capacity of the warmer air. Altered precipitation patterns and increased evaporation lead to increased drought frequency and severity (Dai, 2013). Water availability has been identified as one the most significant factors determining the global sensitivity of vegetation productivity to climate variability (Seddon et al., 2016), thus, major shifts in vegetation patterns can be expected during the following decades affecting food security and terrestrial carbon uptake (Beer et al., 2010; Wheeler and von Braun, 2013). Understanding the effects of altered water availability requires accurate modelling of plant hydraulics at several scales. The development of such models requires rigorous parametrization and careful testing against observations; thus, multi-scale observations of plant water relations are urgently needed (Konings et al., 2019). A wider availability of plant water measurements would also improve our ability to understand and anticipate drought-induced mortality in plants (Martinez-Vilalta et al., 2019).

There are various methods that can be used to measure plant and leaf water status which are based on remote sensing or in-situ measurements. In-situ measurements are either destructive, such as leaf sampling to measure leaf water content or leaf water potential (Ψ_L), or indirect, such as the measurement of subtle changes in xylem or stem diameter with linear transducers (De Swaef et al., 2015) which have been shown to correlate with Ψ_L (Cochard et al., 2002; Dietrich et al., 2018). Ψ_L is one of the most common metric used in plant physiology and ecology to measure plant water status as it describes the sensitivity of plant metabolic and transport processes to decreasing soil water availability and atmospheric evaporative demand. It is still mostly measured manually using a Scholander pressure chamber (Scholander et al., 1965), which is laborious to use, requires access to the canopy and provides only a single reading in time and space of the canopy water status. Also, heterogeneity of Ψ_L within the tree canopy due to variation in illumination can decrease the accuracy of the measurement. To further understand the movement of water within the soil-plant-atmosphere continuum and how the water relations of trees and forests are affected by environmental conditions, non-destructive and reproducible measurement methods capable of providing extensive spatiotemporal information on Ψ_L are urgently needed. Measuring the variation in stem or xylem diameter can provide an assessment of the plant water content and Ψ_L of trees (Dietrich et al., 2018) but cannot capture variation in leaf water content within tree canopies and demands a lot of infrastructure for measuring many trees at the same time.

Remote sensing methods can be used to estimate leaf water content, from which Ψ_L can be estimated as these two are closely related (Cohen et al., 2005; Cotrozzi et al., 2017; Penuelas et al., 1997). Ψ_L can be divided into three different components according to Equation 1, where Ψ_π is the osmotic potential (affected by sugars and other dissolved solutes), Ψ_P is the pressure potential which is tightly linked to relative water content and Ψ_g is the gravitational potential that is especially affecting tall trees. Osmotic potential changes in shorter time intervals due to

Preprints (www.preprints.org) | NOT PEER-REVIEWED | Posted: 26 May 2020 doi:10.20944/preprints202005.0426.v1

changes in solute and water content, and in longer time intervals due to drought or cold acclimation driven by active osmoregulation. Gravitational potential is constant at a given location in a tree canopy, thus, Ψ_L is mainly controlled by changes in the relative water content of leaves within short time intervals such as days (Kubiske and Abrams, 1991; Olsson and Milthorpe, 1983). Thus, by measuring the change in leaf water content, one is able to use that as a proxy for estimating Ψ_L.

$$\Psi_L = \Psi_\pi + \Psi_P + \Psi_g \quad (1)$$

Ψ_L varies during the course of a day and also seasonally. During summer when day temperatures are high, Ψ_L can vary from being near 0 before sunrise to ~ -3 MPa at midday in most tree species the availability of water in the soil is good (Klepper, 1968; Syvertsen and Levy, 1982). Ψ_L has shown also vertical variation e.g. for peach trees (*Prunus* sp.) with height of less than 5 m (Olsson and Milthorpe, 1983) and Norway spruce (*Picea abies* (L.) H. Karst.) trees less than 10 m (Hellkvist et al., 1974). Lower water potentials were detected higher in the canopy likely due to increased transpiration and longer transport distance to the upper parts of the crown (Olsson and Milthorpe, 1983).

Passive remote sensing sensors have been used to measure the variation of leaf water content of individual leaves at close-range, and of canopies using airborne sensors (Colombo et al., 2008; Danson et al., 1992; Penuelas et al., 1997). The estimation of leaf water content using spectral information is often based on the sensitivity of shortwave infrared (SWIR) region (1200-2200 nm) to leaf water content (Ceccato et al., 2001). However, also the near-infrared (NIR) region (700-1000 nm) has been found sensitive to leaf water content (Penuelas et al., 1997). These methods are, however, dependent on solar illumination and therefore cannot be used at very low sun angles or during night to capture the entire diurnal cycle of plant water dynamics. Also, these methods lack the capability to measure within tree variation of leaf water content.

The estimation of Ψ_L has been studied using leaf spectroscopy during the last decade, but mainly focusing on grapevines (*Vitis vinifera* L.) (Bei et al., 2011; Rallo et al., 2014; Santos and Kaye, 2009). Cotrozzi et al. (2017) studied the estimation of predawn Ψ_L using spectroscopic measurement from oak tree leaves (*Quercus oleoides* Schltdl. & Cham.) and detected drought-induced changes in predawn Ψ_L. They found that the most significant spectral features for estimating predawn Ψ_L were in the 1400–1470 nm, 1655–1675 nm, 1840–1950 nm, and 2125–2400 nm regions. Rallo et al. (2014) found that vegetation indices combining bands in NIR region (710-760 nm) and SWIR region (1550-1650 nm) provided the most accurate estimates of Ψ_L. The issue with such methods based on single leaf measurements is that they are prone to error due to the low number of samples and require access to the canopy. Other remote sensing methods that have been used to estimate Ψ_L include thermal remote sensing (Baluja et al., 2012). Cohen et al. (2005) used a thermal camera to assess Ψ_L of cotton plants (Gossypium arboreum L.) and found a strong correlation (Coefficient of determination (R^2) = 0.79) between leaf temperature and Ψ_L using a wet reference target. The leaf temperature increased with decreasing Ψ_L. However, methods based on thermal imaging are dependent on sunlight and thus, not suitable for capturing diurnal variation in Ψ_L.

Preprints (www.preprints.org) | NOT PEER-REVIEWED | Posted: 26 May 2020 doi:10.20944/preprints202005.0426.v1

Terrestrial laser scanning (TLS), is a measurement method that can accurately capture the three dimensional (3D) structure of trees (Dassot et al., 2011; Krooks et al., 2014). A single TLS scan, which typically takes 3-10 min, produces a point cloud of the surroundings ranging from few meters to tens of meters. It is repeatable and allows the measurement of multiple tree canopies in high detail. TLS has been widely used to estimate various variables in forests, e.g., forest structural attributes, leaf area index, wood quality, biomass and quantify dead wood pools (Antonarakis et al., 2010; Kankare et al., 2013; Liang et al., 2014; Pyörälä et al., 2018; Yrttimaa et al., 2019).

In addition to the 3D structure, TLS measures the strength of the backscattered light at the used wavelength, which is commonly referred to as intensity in the literature (Kaasalainen et al., 2011). TLS intensity data can provide additional information on target properties due to its relationship with reflectance at the narrow band of the laser light (Kaasalainen et al., 2009). TLS utilizes an active and controlled source of light that is independent of external illumination reducing the factors that are affecting the measured spectra and allowing for measurements at any time of the day. Dual-wavelength TLS (DW-TLS) and hyperspectral TLS instruments can measure multiple wavelengths enabling the calculation of spectral ratios similar to passive multispectral imaging. Spectral ratios can help reducing the leaf structural effects on the measured reflectance (Junttila et al., 2019, 2016; Nevalainen et al., 2014).

A single intensity measurement consists of the backscattered light under the footprint of the laser, which typically varies around 4-10 mm in a forest environment depending on the distance of the target. TLS intensity measurements are complicated by target geometry, which influences the intensity-distance relationship. TLS intensity can be described using the radar equation, which states that transmitted power (P_t), aperture area (D), optical efficiency (Q), laser-beam divergence (β), atmospheric transmission losses (T), range (R), and backscattering target cross-section (σ) all affect received power (P_r):

$$P_r = \frac{P_t D Q}{4\pi\beta^2} T^2 \frac{\sigma}{R^4} \quad (2)$$

where σ comprises target reflectance, geometry, and illuminated area. The power of R is, however, influenced by target size. Planar targets that cover the entire laser footprint cause a stronger backscatter which diminishes less with distance than linear or blob-like targets due to spherical losses (Wagner et al., 2006). This is an issue with coniferous species since the needles do not cover even the small footprint of TLS causing complications in the distance calibration of intensity data (Junttila et al., 2019; Korpela, 2017).

A clear linkage between leaf water content, measured as equivalent water thickness (EWT), and TLS intensity has been shown in several studies (Elsherif et al., 2019a; Gaulton et al., 2013; Junttila et al., 2018, 2016). Reflectance at the 1550 nm wavelength, which is often utilized in TLS sensors, increases as the leaf water content decreases (Junttila et al., 2016; Rallo et al., 2014). Another wavelength is often employed for accounting leaf structural effects on the measured intensity at 1550 nm, such as 808 nm or 905 mn wavelength, which are assumed to be less sensitive to leaf water content (Elsherif et al., 2018; Junttila et al., 2018). A nearly linear

Preprints (www.preprints.org) | NOT PEER-REVIEWED | Posted: 26 May 2020 doi:10.20944/preprints202005.0426.v1

relationship was found between EWT and a normalized difference index (NDI) calculated from TLS intensity at 1550 nm and 690 nm wavelengths in a drying experiment in a laboratory environment with five species (Junttila et al., 2016). A combination of 905 nm and 1550 nm wavelengths showed a better accuracy than 690 nm and 1550 nm wavelengths in predicting EWT in a greenhouse experiment with Norway spruce seedlings (Junttila et al., 2018). Field experiments with DW-TLS have shown promising results for estimating EWT in deciduous species, but a low prediction accuracy for coniferous species due to the complications arising from distance calibration issues explained above (Elsherif et al., 2019b; Junttila et al., 2019). Elsherif et al. (2019a) investigated the detection of changes in EWT during and after an intense drought event using two observation points in time and DW-TLS data at 808 nm and 1550 nm wavelengths. However, there is still limited understanding on the capability of TLS intensity in characterizing short-term changs in leaf water content that are related to the diurnal cycle of Ψ_L. Research on monitoring of changes in leaf water content using TLS has been limited so far.

To increase our understanding of water dynamics and diurnal variation of Ψ_L within single trees and to overcome the temporal and spatial limitations of passive remote sensing methods and issues arising from the TLS intensity distance calibration of coniferous species, we collected a time series of 15 TLS scans at 905 nm and 1550 nm wavelengths in the field. We studied and scanned three trees of two species with a nearly constant measurement geometry to study the diurnal variation of Ψ_L during a 50 h time period coupled with destructive leaf measurements and radial stem diameter measurements. Since we cannot measure pressure directly, the estimation of Ψ_L is based on the well-established theory that change in leaf water content is the main driver of change in Ψ_L during short time intervals, such as days. Our main research question was to investigate how large part of the diurnal variation in Ψ_L can be captured using TLS intensity observations based on the known correlation between leaf water content, Ψ_L and TLS intensity at 905 nm and 1550 nm wavelengths. Based on the existing knowledge, we hypothesized that there is a correlation between the measured intensity and Ψ_L. This research contributes to increasing the understanding of tree water dynamics and to the development of novel methods to measure and monitor it.

2. Material and Methods

We measured two Scots pines (*Pinus sylvestris* L.) and one Silver birch (*Betula pendula* Roth*)* (Table 1) during a 50 hour monitoring period from the 29th to the 31st of July in 2019 at the Station for Measuring Ecosystem-Atmosphere Relations (SMEAR II) at Hyytiälä Forest Research Station in Juupajoki, Finland (61°46' N, 24°17' E, 170 m a.s.l.) (Table 1). The investigated trees were growing in a 57-year-old Scots pine stand with admixtures of Silver birch, Norway spruce (*Picea abies* (L.) Karst.), rowan (*Sorbus aucuparia* L.), European aspen (*Populus tremula* L.) and Common juniper (*Juniperus communis* L.). The trees were located around a multi-story measurement tower enabling the collection of observations from the tree crowns during the investigation period.

Preprints (www.preprints.org) | NOT PEER-REVIEWED | Posted: 26 May 2020 doi:10.20944/preprints202005.0426.v1

Radial stem variation of the trees was measured with point dendrometers, i.e. linear variable displacement transducers (model AX/5.0/S, Solartron Inc. West Sussex, U.K.) at a height of 1.5 m. The dendrometers measured the radial variation of the stem and xylem separately. The xylem diameter changes due to reversible changes in xylem content, while the stem diameter changes due to both reversible changes in stem water content and due to irreversible cell enlargement associated with cambial growth (Chan et al., 2016; Dietrich et al., 2018). As the investigation period was late summer, the cell enlargement phase of cambial growth of the stem had almost ceased (see Chan et al. (2016) for the phenology of growth at the site). The radial stem measurements were recorded continuously at a one-minute time resolution.

Environmental variables, such as temperature, relative humidity, wind speed, wind direction and the amount of incoming thermal radiation, were measured from a measurement tower located at about 50 meters from the measurement site (Figure 1). The measurements were conducted in one-minute intervals. Soil water potential was simultaneously measured with tensiometers (EQ2 Equitensiometer, Delta-T) combined to pressure transducers (TR2000A, Trans Instruments) at the depths of five and 15 cm at 15 minute intervals. The data described here are openly accessible from the SMEAR station database (https://avaa.tdata.fi/web/smart/smear).

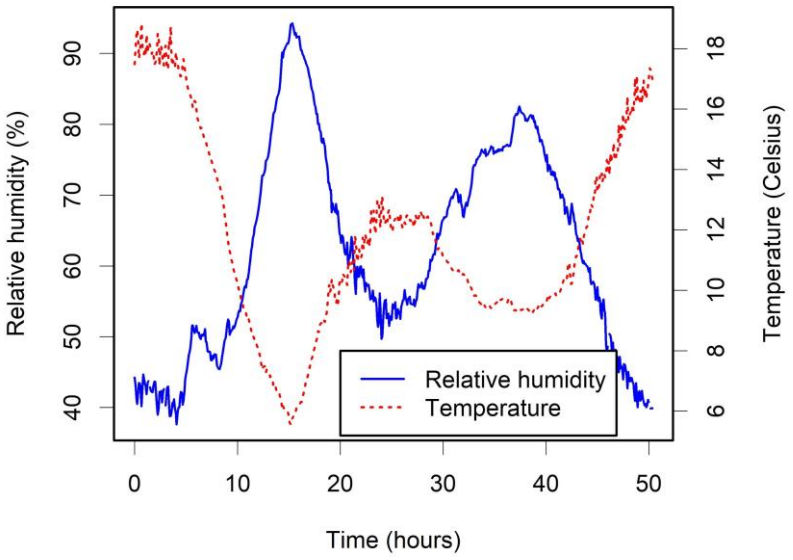

Figure 1. Variation of temperature and relative humidity during the monitoring period. The measurements were started at 1 pm on the 29th of July and ended at 3 pm on the 31st of July 2019.

Preprints (www.preprints.org) | NOT PEER-REVIEWED | Posted: 26 May 2020 doi:10.20944/preprints202005.0426.v1

Table 1. Diameter at breast height (DBH) and height of the investigated trees.

	Scots pine 1	**Scots pine 2**	**Silver birch**
DBH (cm)	22.5	19.8	20.1
Height (m)	18.9	19.5	20.6

2.1 TLS measurements

The TLS measurements were started at 13:00 on the 29th of July and ended at 15:00 in the afternoon two days later. During this monitoring period the trees were scanned 15 times using two scanners utilizing wavelengths at 905 nm and 1550 nm. Each tree was measured with a single scan subsequently with both scanners from the position with clear visibility to the tree crown to avoid occlusion caused by other trees. The distance to the trees varied from 11 m to 13 m. The time difference between the consecutive two scans was approximately 15 minutes. The scanners used were a FARO X330 (FARO Europe GmbH & Co. KG, Korntal-Münchingen, Germany), which operates at 1550 nm, and a Trimble TX5 (Trimble Inc., Sunnyvale, CA, USA) operating at 905 nm wavelength. These scanners have similar technical specifications: beam divergence of 0.19 mrad, a max scan rate of 976 kHz, and intensity recording to a digital number (-2048 to 2033). The beam diameter at output differs slightly FARO X330 having a beam diameter of 2.25 mm and the Trimble TX5 of 3 mm. Both scanners utilize phase shifting range measurements. The scanners have the same boxing; thus, the viewing angle is the same between the scanners. Both scanners' resolutions were set to 0.5, resulting in a vertical spacing of 3.07 mm at a 10 m distance; the quality parameter was set to 2× (i.e., two measurements were made for each point, and the resulting value was the mean of the two). We placed 11 target spheres (each of diameter 145 mm) around the measurement tower for further scan registration. A Lambertian Spectralon reflectance panel (Labsphere, North Sutton, NH, USA) with a nominal reflectance of 40% was used as a reference target at a constant distance to normalize the laser intensity of each scan.

2.2 Leaf water potential measurements

Ψ_L was measured at 9-time intervals during the monitoring period. The top of the tree canopies was divided into three height bins for Ψ_L measurements to ensure a reliable reference for entire tree canopies: the top 2 m, 2-4 m from the top and 4-6 m from the top. The Ψ_L samples were collected at the same time with the TLS measurements. Each sample consisted of four needles or leaves that were collected to air tight plastic bags, stored in a dark and cool bag and carried immediately to the nearby laboratory, where Ψ_L was measured using a Scholander pressure chamber (PMS-1000; PMS Instruments, Albany, OR, USA). Each Ψ_L measurement was the mean of the four samples.

Preprints (www.preprints.org) | NOT PEER-REVIEWED | Posted: 26 May 2020 doi:10.20944/preprints202005.0426.v1

Since it is known that there is a dependency between canopy water status and radial stem diameter variation (Dietrich et al., 2018), we created linear regression models between Ψ_L and the radial stem diameter variation for each tree to increase the number of Ψ_L data points. Using these models, we predicted Ψ_L for each 15 time points of TLS data. Because there is a lag after a change of Ψ_L in the change in radial stem diameter, we used a lag in creating the regression models (Sevanto et al., 2002). The predicted Ψ_L is abbreviated as $\Psi_{P\text{-}L}$ in the text.

2.3 Point cloud processing

The point clouds from each measurement location were co-registered to a common arbitrary coordination system using the external sphere targets as reference points. The registration was performed in FARO Scene point cloud processing software. Each tree was then manually delineated from the individual point clouds using the CloudCompare software package (version 2.10) (Dewez et al., 2016). The calibration of intensity was conducted to reduce variation caused by factors such as distance. The intensity correction workflow followed the procedure presented in Junttila et al. (2019), which included distance and logarithmic corrections and the normalization of intensity with a reflectance panel with known reflectance. The distance correction was done using a 10^{th} degree polynomial function that was modeled with empirical data of intensity and distance of the scanner. The raw intensity scale of the scanner was found logarithmic. Thus, a linearization of the intensity scale was necessary using empirical relationships between reflectance and raw intensity. Further details are provided in Junttila et al. (2019).

2.4 Point cloud segmentation

The canopy of each tree was segmented from the point clouds to include mainly needle or leaf points into the analysis. The segmentation was based on a minimum height that was determined visually. The minimum heights that were used to segment the canopies were 9.9 m, 11.5 m and 10 m, for the pine 1, the pine 2 and the birch, respectively. We included all the points from the canopy into the analysis to avoid interfering with the intensity data distribution at the tree-level and to ensure consistency of the data between subsequent measurements of the time-series. Thus, no classification to branch and needle or leaf points was carried out. The number of points in the resulting point clouds, which were used in the analysis, varied between 220,000 and 450,000 between the trees and observation times.

2.5 Explanatory intensity metrics

A variety of intensity metrics was calculated for each segmented point cloud (Table 2). These metrics describe the distribution of intensity values within a given point cloud at different wavelengths. The metrics were calculated for the 905 and 1550 nm wavelengths separately. Since the calculation of NDI for single 3D points was complicated due to slight movement of branches between the consecutive scans, NDI was calculated based on the distribution of intensity values in the canopy. The calculation of NDI was done using the percentiles (10^{th},

Preprints (www.preprints.org) | NOT PEER-REVIEWED | Posted: 26 May 2020 doi:10.20944/preprints202005.0426.v1

20th, 30th… 90th) and the mean of 905 nm and 1550 nm wavelengths (Equation 3). All the intensity metrics are used in Table 2.

$$NDI = \frac{I_{905} - I_{1550}}{I_{905} + I_{1550}} \quad (3)$$

Table 2. Description of the calculated intensity metrics. In the table, i denotes the wavelength followed by the name of the metric. For example "1550_mean" means average intensity at the 1550 nm wavelength. Respectively, normalized difference index (NDI) metrics are followed by the percentile used in the calculation of NDI. For example, "NDI_p20" means that metric has been calculated using the 20th percentile of 905 nm and 1550 nm wavelengths).

Metric	**Description**
i_mean	Average intensity
i_std	Standard deviation of intensity
i_p10, i_p20, … i_p90	Multiple-of-10 percentiles (10th through 90th) of the intensity distribution
i_max	Maximum intensity
i_min	Minimum intensity
i_kur	Kurtosis of the intensity distribution (Davies and Goldsmith, 1976)
i_ske	Skewness of the intensity distribution (Davies and Goldsmith, 1976)

Preprints (www.preprints.org) | NOT PEER-REVIEWED | Posted: 26 May 2020 doi:10.20944/preprints202005.0426.v1

i_entropy	Shannon diversity index (entropy) of the intensity distribution (Shannon, 2001)
i_range	Difference between maximum and minimum intensity
i_D05, i_D25, i_D50, i_D75	Density variables: the 95^{th} percentile divided by 5^{th}, 25^{th}, 50^{th}, and 75^{th} percentiles, respectively.

2.6 Statistical analysis

Student's two-sided *t*-tests were used to assess the difference in Ψ_L at different heights. Linear regression modeling was used to assess the relationships between the intensity metrics and Ψ_L. Regression models were created using both the measured and the predicted Ψ_L as dependent variables. Normality of the data was tested using the Shapiro-Wilkinson test (Hanusz and Tarasińska, 2015). Coefficient of determination (R^2) and Root-mean-square-error (RMSE) were calculated to assess the estimation accuracy of the intensity variables. All of the statistical analysis was carried out within the R package (R. Core Team, 2015).

3. Results

3.1 Variation of leaf water potential based on the Scholander pressure chamber

The lowest Ψ_L values were observed on the day the measurements were started (Figure 2). From the Figure 2, one can observe that the Silver birch shows a minor trend of decreasing Ψ_L higher in the tree, but no significant differences in Ψ_L between the different height layers were observed during the monitoring period. Soil water potential varied between -0.05 and -0.08 MPa at the 15 cm depth, and between -0.15 MPa and -0.21 MPa at the 5 cm depth.

Preprints (www.preprints.org) | NOT PEER-REVIEWED | Posted: 26 May 2020 doi:10.20944/preprints202005.0426.v1

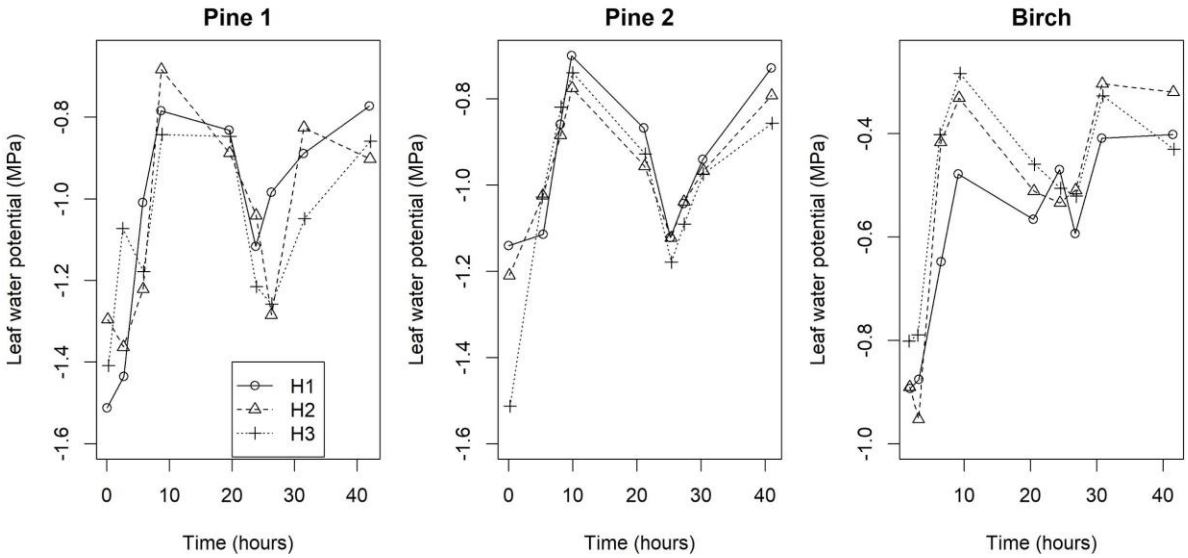

Figure 2. Variation of leaf water potential (Ψ_L) at different heights during the monitoring period. H1 denotes the top 2 m of height, H2 the top 2-4 m of height and H3 the top 4-6 m of height. The measurements were started at 1 pm on the 29th of July and ended at 3 pm on the 31st of July 2019.

3.2 Leaf water potential prediction based on the stem diameter measurements

A strong linear relationship was observed between Ψ_L and stem diameter variation for each tree (Figure 3). The relationship was found the strongest by using a 90-minute time lag between the Ψ_L and stem diameter measurement.

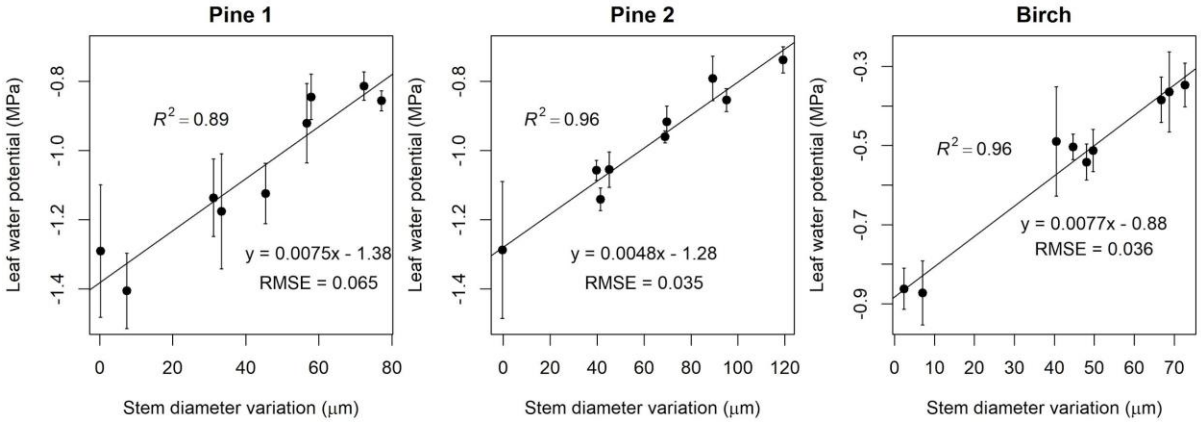

Figure 3. The relationship between leaf water potential (Ψ_L) and stem diameter variation. The error bars represent the standard deviation of the Ψ_L measurements from different heights. Coefficient of determination (R^2) and root-mean-square-error (RMSE) for the prediction models are also presented.

Preprints (www.preprints.org) | NOT PEER-REVIEWED | Posted: 26 May 2020 doi:10.20944/preprints202005.0426.v1

3.3 Assessing the relationships between leaf water potential and intensity metrics

The intensity metrics explained a significant proportion of the variation in Ψ_L (Figure 4). The best predicting variables (905_p20, 905_p60, 905_min) explained 72%, 73% and 79% of the variation in Ψ_L in the pine 1, pine 2 and the birch, respectively (Table 3). Generally, the strongest predictors were mainly distribution features of the 905 nm wavelength, but for pine 1 the distribution of 1550 nm showed similar explanatory power. The D25 intensity feature of 905 nm wavelength explained 78% of the variation in Ψ_L with observations from all of the trees in the prediction model. However, one must notice that the distribution of intensity metrics using observations from all of the trees in the same model were not normally distributed, which is against the assumptions of linear regression, causing likely overestimation of the relationship. This was due to the uneven distribution of tree species in the samples.

Table 3. The five strongest predictors, coefficient of determination (R^2) and root-mean-square-error (RMSE, MPa) for the linear regression models explaining leaf water potential (Ψ_L) using intensity metrics for each tree and all trees together. In these prediction models, Ψ_L and TLS intensity were measured in nine observation points in time. Description of the predictors is provided in Table 2.

Pine 1			**Pine 2**			**Birch**		
Predictor	R^2	*RMSE*	*Predictor*	R^2	*RMSE*	*Predictor*	R^2	*RMSE*
905_p20	0.72	0.106	905_p60	0.73	0.085	905_min	0.79	0.082
1550_p60	0.68	0.114	905_p50	0.73	0.086	905_p10	0.65	0.106
905_p30	0.68	0.114	905_p40	0.73	0.086	905_D25	0.59	0.114
1550_p70	0.66	0.118	905_mean	0.69	0.092	1550_min	0.57	0.117
1550_p80	0.61	0.126	905_p70	0.69	0.093	905_entropy	0.57	0.118
All trees								
Predictor			R^2			*RMSE*		
905_D25			0.78			0.137		
905_D05			0.63			0.179		
905_std			0.63			0.179		

905_D50	0.6	0.185
905_p90	0.59	0.188

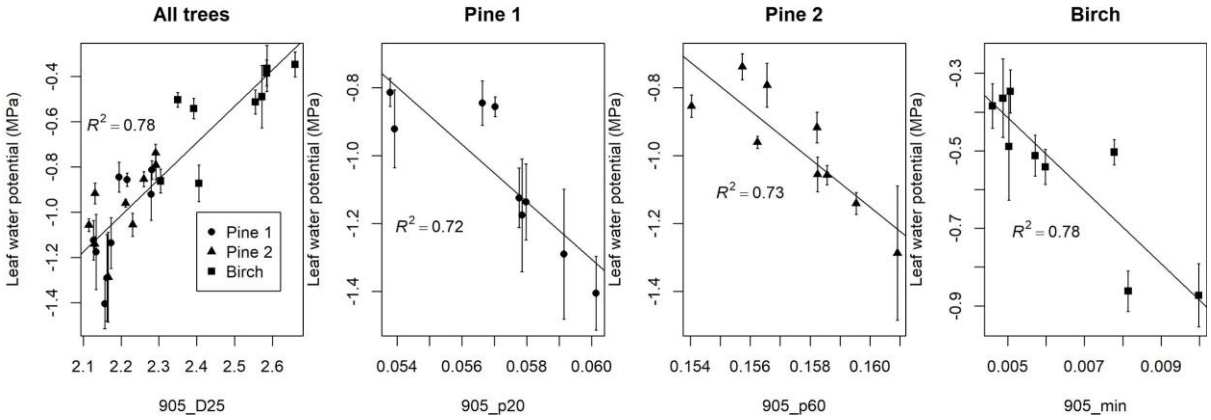

Figure 4. The relationship and coefficient of determination (R^2) between leaf water potential (Ψ_L) and intensity metrics for all trees and for each tree separately. The error bars represent the standard deviation of measured Ψ_L at different heights. Description of the predictors 905_D25, 905_p20, 905_p60 and 905_min is provided in Table 2.

3.4 Assessing the relationships between predicted leaf water potential and intensity metrics

When we predicted Ψ_L to all of the 15 observation points in time (See 3.2) and used $\Psi_{P\text{-}L}$ as a dependent variable in our linear regression models, we obtained similar results that were presented in 3.3. On average, the 905 nm wavelength features showed to be able to explain a larger proportion of the variation in predicted Ψ_L than 1550 nm and NDI features with the exception of Pine 1 (Table 4, Figure 5). For the birch, the lowest part of the 905 nm intensity distribution showed to be the most sensitive to variation in Ψ_L with the 905_min, 905_p05 and 905_p10 features among the strongest predictors. Whereas for the pines, the strongest predictors varied around the mean of the intensity distribution (i.e., p30, p40, p50, p60 features). Again one must note that, the intensity variables of all the trees pooled together were not normally distributed according to the Shapiro-Wilkinson test due to different amounts of pines and birch in the data.

Table 4. The five strongest predictors, coefficient of determination (R^2) and root- mean-square-error (RMSE, MPa) for the linear regression models explaining predicted leaf water potential ($\Psi_{P\text{-}L}$) using intensity metrics for each tree and all trees together. In these prediction models, Ψ_L is estimated to 15 observation points in time and the TLS intensity are measured from the respective time points. Description of the predictors is provided in Table 2. Note that the predictor 905_D25 is transformed using the logarithm (log(905_D25)).

Preprints (www.preprints.org) | NOT PEER-REVIEWED | Posted: 26 May 2020 doi:10.20944/preprints202005.0426.v1

Pine 1			**Pine 2**			**Birch**		
Predictor	R^2	*RMSE*	*Predictor*	R^2	*RMSE*	*Predictor*	R^2	*RMSE*
1550_p50	0.61	0.162	905_p40	0.62	0.132	905_min	0.76	0.105
905_D75	0.59	0.166	905_entropy	0.62	0.132	905_p05	0.68	0.121
1550_p40	0.58	0.166	905_mean	0.61	0.134	905_p10	0.66	0.125
1550_p30	0.56	0.171	905_p30	0.61	0.134	905_entropy	0.66	0.124
1550_p60	0.56	0.171	1550_D50	0.59	0.137	905_p20	0.56	0.142

All trees		
Predictor	R^2	*RMSE*
log(905_D25)	0.73	0.173
905_D50	0.56	0.221
905_D05	0.54	0.225
905_std	0.54	0.226
NDI_p90	0.53	0.228

Preprints (www.preprints.org) | NOT PEER-REVIEWED | Posted: 26 May 2020 doi:10.20944/preprints202005.0426.v1

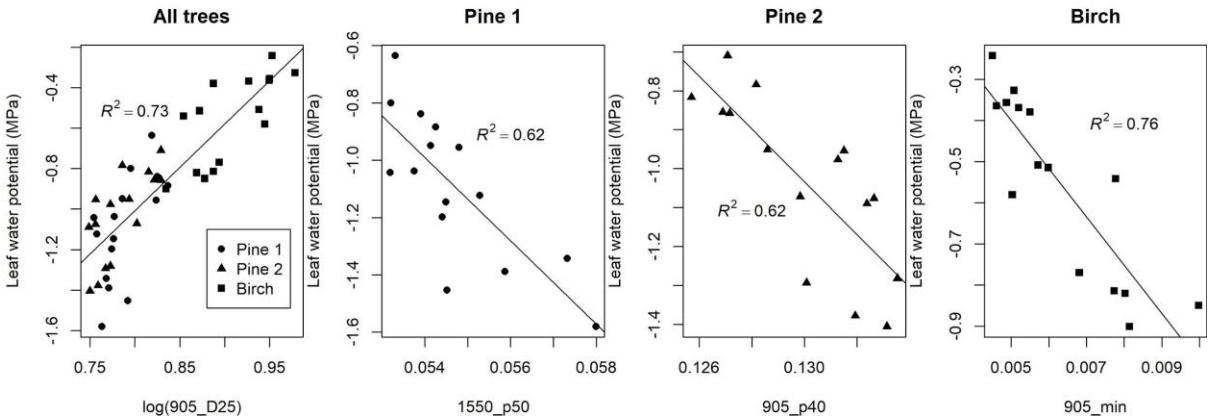

Figure 5. The relationship and coefficient of determination (R^2) between predicted leaf water potential ($\Psi_{P\text{-}L}$) and laser intensity metrics for all trees and for each tree separately. Description of the predictors 905_D25, 1550_p50, 905_p40, 905_min is provided in Table 2. Prefix log indicates that the predictor has been transformed using the logarithm function.

4. Discussion

The main aim of this study was to investigate how much of the diurnal variation in Ψ_L within Scots pine and Silver birch trees can be explained using TLS intensity measurements. Our results showed that a time-series of TLS intensity measurements can capture from 62 % to 78 % of the variation in Ψ_L. Our destructive Ψ_L measurements were complemented with estimated Ψ_L values that were based on stem diameter change measurements and existing knowledge on the time lag between the change in Ψ_L and stem diameter (Lintunen et al., 2020). The time lag of 90 minutes that we used is in line with earlier results (Sevanto et al., 2002).

TLS intensity showed a relatively strong relationship with Ψ_L (R^2 of 0.61-0.79), especially at the 905 nm wavelength (See Table 3). This strengthens the existing knowledge as it has been observed that this part of the spectra is sensitive to variation in relative water content which is directly linked to variation in Ψ_L (Penuelas et al., 1997). It seems that TLS intensity is capable of capturing subtle variation in leaf reflectance that occurs within a 24 hour period due to changes in leaf water content. Based on the observed relationship between Ψ_L and TLS intensity in the field, TLS intensity measurements seemed relatively insensitive to the constantly varying illumination conditions that, based on previous research, are hindering the use of passive remote sensing methods for many forest monitoring applications (Cheng et al., 2014; Nichol et al., 2006).

When estimating Ψ_L , there were differences in the performance of the intensity metrics between the tree species. For the Scots pines, the intensity metrics that were strongest predictors in explaining variation in Ψ_L, were found around the middle of the intensity distribution at both 905 nm and 1550 nm wavelengths varying between the 20th and the 60th percentile of the distribution. For the Silver birch, the intensity metrics that were strongest predictors in explaining variation in Ψ_L were in the lowest part of the intensity distribution of both 905 nm

Preprints (www.preprints.org) | NOT PEER-REVIEWED | Posted: 26 May 2020 doi:10.20944/preprints202005.0426.v1

and 1550 nm wavelengths, 905 nm wavelength showing a distinctly better performance. The differences in the intensity metrics explaining the variation in Ψ_L between trees are likely due to the varying structure of the tree crowns, difference in leaf shape (coniferous vs. deciduous) and differences in the amount of needle/leaf and stem/branch points in the segmented point cloud. The narrow leaf width of coniferous species causes spherical losses resulting in a weaker backscattered intensity from the needles (Korpela, 2017). Therefore the difference in backscattered intensity between stem or branch points and foliage points is greater for coniferous species. The differences in the leaf shape and the resulting effect on backscattered intensity likely explain why the intensity features differed between the two species.

Our preliminary tests indicated that filtering of stray points and detailed segmentation of the point clouds caused the relationship between intensity and Ψ_L to substantially decrease, which was likely due to the effect of these procedures on the intensity distribution. Therefore, we suggest that one should very critically evaluate the effect of point cloud filtering, segmentation and classification on the intensity of the resulting point clouds, when using intensity as the main source of information and especially when using a time-series of intensity observations, as was used in this study.

We used a simple segmentation of the canopy and did not separate leaf and stem points in this study. We also did not filter stray or "ghost" points that commonly result from the laser hitting the edges of a target (Eitel et al., 2010). Although, one could expect that the classification of leaf material could improve the estimation accuracy of Ψ_L, the correlation between TLS intensity metrics and Ψ_L was already strong using the methods that were applied in this study. One should be careful to not affect the intensity distribution, when adding methods such as classification of leaves or filtering of stray points to the processing pipeline. Our results are likely influenced by the large amount of intensity observations from each tree canopy, which is resulting in a more stable intensity distribution than what would be possible to achieve for individual branches or leaves. The trees were also scanned each time from the same position, which in principle should result in a nearly equal amount of stem and leaf points in the point clouds.

Earlier studies have found that NDI metrics have been stronger predictors for EWT than single wavelength metrics (Elsherif et al., 2019b; Junttila et al., 2019, 2018). In this study, the NDI metrics did not provide any improvement compared to single wavelength metrics in estimating Ψ_L. The differences in the design of this and other experiments may have caused this. The main differences compared to previous studies were: 1) the utilization of a dense time-series to monitor diurnal variation in leaf water status instead of single observations of different leaves or trees, 2) non-destructive nature of the research design (i.e., same trees were measured multiple times) and 3) the estimation of Ψ_L instead of EWT. Thus, direct comparisons to previous studies should not be made. The reason why the NDI metrics did not perform as well as single wavelength metrics in the estimation of Ψ_L was likely caused by, firstly, the nearly constant leaf/needle structure during the monitoring period, which reduces the need for leaf structural normalization with NDI metrics (Junttila et al., 2018). Single wavelength metrics have been strong predictors of EWT for single species in a drying experiment (Junttila et al.,

2016). Structural differences in foliage have a greater effect on intensity if a larger amount of trees are monitored simultaneously. Secondly, slight movement of leaves and branches occured between the subsequent scans at the 905 nm and 1550 nm wavelengths, which could affect the stability of the NDI metrics through the time-series. Thirdly, we were using TLS intensity to measure the change in leaf water content and to derive Ψ_L instead of direct estimation of EWT.

TLS intensity measurements require calibration (Kaasalainen et al., 2011, 2009). The lack of reliable calibration methods is hindering use of intensity information. The current calibration methods are unable to take into account the differences in the backscattered reflectance that are caused by small targets that do not cover the laser footprint entirely. However, based on the results of this study and earlier work (Junttila et al., 2019), TLS intensity measurements from tree crowns can reveal changes caused by e.g. altered water content despite the challenges in the calibration.

However, in our controlled experiment, TLS intensity showed to be able to explain 61%-78% of the within tree and between tree variation in Ψ_L. The best performing intensity features were mainly density features of the 905 nm wavelength (905_D25, 905_D05, 905_D50) that describe the variation in the TLS intensity within a tree canopy. In other words, the changes in the shape of the intensity distribution due to varying Ψ_L have been similar between trees and tree species encouraging for further studies towards developing a general model that could estimate Ψ_L using TLS intensity measurements. It should be noted that the amount of trees and samples were rather limited in this study for evaluating the capability of TLS intensity time-series in estimating Ψ_L for trees of varying ages, species and structures growing in various ecoregions, but based on the results of this study, it seems that there is a clear correlation between TLS intensity and Ψ_L.

The used estimation approach is based on the relationship between Ψ_L and relative water content. However, the relative water content, is not the only variable affecting Ψ_L and especially at longer time intervals or during extreme events, such as drought, osmotic potential can affect Ψ_L as well (Bartlett et al., 2012; Nobel, 1999). Therefore, on longer time intervals (e.g. month, season, year) the estimation accuracy of Ψ_L using TLS intensity is likely constrained by the influence of changes in osmotic potential.

We investigated the capability of TLS intensity in capturing the diurnal variation of Ψ_L. Earlier studies that have utilized TLS intensity in plant water status estimation have concentrated on estimating EWT, which can have large variation within tree canopies and is strongly related to leaf mass per area (LMA). LMA varies greatly between species and within species depending on environmental conditions, such as light and temperature (Poorter et al., 2009). Therefore EWT is less useful in understanding the plant water status compared to Ψ_L (Elsherif et al., 2019b; Junttila et al., 2019). Although, intensity metrics explained large part of the variation in Ψ_L in our controlled experiment including three trees, there is still limited knowledge on how consistent is the relation between Ψ_L and intensity metrics within and between the tree communities. Theoretically, TLS can measure tens of tree canopies with a single easy-to-repeat scan and the ability of estimating Ψ_L of those canopies would enable the measurement of Ψ_L at

unprecedented spatial and temporal scales, which can help us to further understand the movement of water within the soil-plant-atmosphere continuum and the effect of warmer and drier climate on our ecosystems.

Acknowledgements

This work was supported by the Faculty of Agriculture and Forestry of the University of Helsinki, the Academy of Finland under [grant numbers 307362, 316096/320075, and 330422] and the Finnish Cultural Foundation.

References

Antonarakis, A.S., Richards, K.S., Brasington, J., Muller, E., 2010. Determining leaf area index and leafy tree roughness using terrestrial laser scanning. Water Resources Research. https://doi.org/10.1029/2009wr008318

Baluja, J., Diago, M.P., Balda, P., Zorer, R., Meggio, F., Morales, F., Tardaguila, J., 2012. Assessment of vineyard water status variability by thermal and multispectral imagery using an unmanned aerial vehicle (UAV). Irrigation Science. https://doi.org/10.1007/s00271-012-0382-9

Bartlett, M.K., Scoffoni, C., Sack, L., 2012. The determinants of leaf turgor loss point and prediction of drought tolerance of species and biomes: a global meta-analysis. Ecol. Lett. 15, 393–405. https://doi.org/10.1111/j.1461-0248.2012.01751.x

Beer, C., Reichstein, M., Tomelleri, E., Ciais, P., Jung, M., Carvalhais, N., Rödenbeck, C., Arain, M.A., Baldocchi, D., Bonan, G.B., Bondeau, A., Cescatti, A., Lasslop, G., Lindroth, A., Lomas, M., Luyssaert, S., Margolis, H., Oleson, K.W., Roupsard, O., Veenendaal, E., Viovy, N., Williams, C., Woodward, F.I., Papale, D., 2010. Terrestrial gross carbon dioxide uptake: global distribution and covariation with climate. Science 329, 834–838. https://doi.org/10.1126/science.1184984

Bei, R.D.E., de Bei, R., Cozzolino, D., Sullivan, W., Cynkar, W., Fuentes, S., Dambergs, R., Pech, J., Tyerman, S., 2011. Non-destructive measurement of grapevine water potential using near infrared spectroscopy. Australian Journal of Grape and Wine Research. https://doi.org/10.1111/j.1755-0238.2010.00117.x

Ceccato, P., Flasse, S., Tarantola, S., Jacquemoud, S., Grégoire, J.-M., 2001. Detecting vegetation leaf water content using reflectance in the optical domain. Remote Sensing of Environment. https://doi.org/10.1016/s0034-4257(01)00191-2

Chan, T., Hölttä, T., Berninger, F., Mäkinen, H., Nöjd, P., Mencuccini, M., Nikinmaa, E., 2016. Separating water-potential induced swelling and shrinking from measured radial stem variations reveals a cambial growth and osmotic concentration signal. Plant Cell Environ. 39, 233–244. https://doi.org/10.1111/pce.12541

Cheng, T., Riaño, D., Ustin, S.L., 2014. Detecting diurnal and seasonal variation in canopy water content of nut tree orchards from airborne imaging spectroscopy data using continuous wavelet analysis. Remote Sensing of Environment. https://doi.org/10.1016/j.rse.2013.11.018

Cochard, H., Coll, L., Le Roux, X., Améglio, T., 2002. Unraveling the effects of plant

hydraulics on stomatal closure during water stress in walnut. Plant Physiol. 128, 282–290. https://doi.org/10.1104/pp.010400

Cohen, Y., Alchanatis, V., Meron, M., Saranga, Y., Tsipris, J., 2005. Estimation of leaf water potential by thermal imagery and spatial analysis. J. Exp. Bot. 56, 1843–1852. https://doi.org/10.1093/jxb/eri174

Colombo, R., Meroni, M., Marchesi, A., Busetto, L., Rossini, M., Giardino, C., Panigada, C., 2008. Estimation of leaf and canopy water content in poplar plantations by means of hyperspectral indices and inverse modeling. Remote Sensing of Environment. https://doi.org/10.1016/j.rse.2007.09.005

Cotrozzi, L., Couture, J.J., Cavender-Bares, J., Kingdon, C.C., Fallon, B., Pilz, G., Pellegrini, E., Nali, C., Townsend, P.A., 2017. Using foliar spectral properties to assess the effects of drought on plant water potential. Tree Physiol. 37, 1582–1591. https://doi.org/10.1093/treephys/tpx106

Dai, A., 2013. Increasing drought under global warming in observations and models. Nature Climate Change. https://doi.org/10.1038/nclimate1633

Danson, F.M., Steven, M.D., Malthus, T.J., Clark, J.A., 1992. High-spectral resolution data for determining leaf water content. International Journal of Remote Sensing. https://doi.org/10.1080/01431169208904049

Dassot, M., Constant, T., Fournier, M., 2011. The use of terrestrial LiDAR technology in forest science: application fields, benefits and challenges. Annals of Forest Science. https://doi.org/10.1007/s13595-011-0102-2

Davies, O.L., Goldsmith, P.L., 1976. Statistical Methods in Research and Production.

De Swaef, T., De Schepper, V., Vandegehuchte, M.W., Steppe, K., 2015. Stem diameter variations as a versatile research tool in ecophysiology. Tree Physiol. 35, 1047–1061. https://doi.org/10.1093/treephys/tpv080

Dewez, T.J.B., Girardeau-Montaut, D., Allanic, C., Rohmer, J., 2016. FACETS : A CLOUDCOMPARE PLUGIN TO EXTRACT GEOLOGICAL PLANES FROM UNSTRUCTURED 3D POINT CLOUDS. ISPRS - International Archives of the Photogrammetry, Remote Sensing and Spatial Information Sciences. https://doi.org/10.5194/isprs-archives-xli-b5-799-2016

Dietrich, L., Zweifel, R., Kahmen, A., 2018. Daily stem diameter variations can predict the canopy water status of mature temperate trees. Tree Physiol. 38, 941–952. https://doi.org/10.1093/treephys/tpy023

Eitel, J.U.H., Vierling, L.A., Long, D.S., 2010. Simultaneous measurements of plant structure and chlorophyll content in broadleaf saplings with a terrestrial laser scanner. Remote Sensing of Environment. https://doi.org/10.1016/j.rse.2010.04.025

Elsherif, A., Gaulton, R., Mills, J., 2019a. Four Dimensional Mapping of Vegetation Moisture Content Using Dual-Wavelength Terrestrial Laser Scanning. Remote Sensing 11, 2311. https://doi.org/10.3390/rs11192311

Elsherif, A., Gaulton, R., Mills, J., 2018. Estimation of vegetation water content at leaf and canopy level using dual-wavelength commercial terrestrial laser scanners. Interface Focus 8, 20170041. https://doi.org/10.1098/rsfs.2017.0041

Elsherif, A., Gaulton, R., Shenkin, A., Malhi, Y., Mills, J., 2019b. Three dimensional mapping of forest canopy equivalent water thickness using dual-wavelength terrestrial

laser scanning. Agric. For. Meteorol. 276-277, 107627. https://doi.org/10.1016/j.agrformet.2019.107627

Gaulton, R., Danson, F.M., Ramirez, F.A., Gunawan, O., 2013. The potential of dual-wavelength laser scanning for estimating vegetation moisture content. Remote Sensing of Environment. https://doi.org/10.1016/j.rse.2013.01.001

Hanusz, Z., Tarasińska, J., 2015. Normalization of the Kolmogorov–Smirnov and Shapiro–Wilk tests of normality. Biometrical Letters. https://doi.org/10.1515/bile-2015-0008

Hellkvist, J., Richards, G.P., Jarvis, P.G., 1974. Vertical Gradients of Water Potential and Tissue Water Relations in Sitka Spruce Trees Measured with the Pressure Chamber. The Journal of Applied Ecology. https://doi.org/10.2307/2402215

Junttila, S., Holopainen, M., Vastaranta, M., Lyytikäinen-Saarenmaa, P., Kaartinen, H., Hyyppä, J., Hyyppä, H., 2019. The potential of dual-wavelength terrestrial lidar in early detection of Ips typographus (L.) infestation – Leaf water content as a proxy. Remote Sensing of Environment. https://doi.org/10.1016/j.rse.2019.111264

Junttila, S., Sugano, J., Vastaranta, M., Linnakoski, R., Kaartinen, H., Kukko, A., Holopainen, M., Hyyppä, H., Hyyppä, J., 2018. Can Leaf Water Content Be Estimated Using Multispectral Terrestrial Laser Scanning? A Case Study With Norway Spruce Seedlings. Front. Plant Sci. 9, 299. https://doi.org/10.3389/fpls.2018.00299

Junttila, S., Vastaranta, M., Liang, X., Kaartinen, H., Kukko, A., Kaasalainen, S., Holopainen, M., Hyyppä, H., Hyyppä, J., 2016. Measuring Leaf Water Content with Dual-Wavelength Intensity Data from Terrestrial Laser Scanners. Remote Sensing. https://doi.org/10.3390/rs9010008

Kaasalainen, S., Hyyppa, H., Kukko, A., Litkey, P., Ahokas, E., Hyyppa, J., Lehner, H., Jaakkola, A., Suomalainen, J., Akujarvi, A., Kaasalainen, M., Pyysalo, U., 2009. Radiometric Calibration of LIDAR Intensity With Commercially Available Reference Targets. IEEE Transactions on Geoscience and Remote Sensing. https://doi.org/10.1109/tgrs.2008.2003351

Kaasalainen, S., Jaakkola, A., Kaasalainen, M., Krooks, A., Kukko, A., 2011. Analysis of Incidence Angle and Distance Effects on Terrestrial Laser Scanner Intensity: Search for Correction Methods. Remote Sensing. https://doi.org/10.3390/rs3102207

Kankare, V., Räty, M., Yu, X., Holopainen, M., Vastaranta, M., Kantola, T., Hyyppä, J., Hyyppä, H., Alho, P., Viitala, R., 2013. Single tree biomass modelling using airborne laser scanning. ISPRS Journal of Photogrammetry and Remote Sensing. https://doi.org/10.1016/j.isprsjprs.2013.08.008

Klepper, B., 1968. Diurnal pattern of water potential in woody plants. Plant Physiol. 43, 1931–1934. https://doi.org/10.1104/pp.43.12.1931

Konings, A.G., Rao, K., Steele-Dunne, S.C., 2019. Macro to micro: microwave remote sensing of plant water content for physiology and ecology. New Phytol. 223, 1166–1172. https://doi.org/10.1111/nph.15808

Korpela, I., 2017. Acquisition and evaluation of radiometrically comparable multi-footprint airborne LiDAR data for forest remote sensing. Remote Sensing of Environment. https://doi.org/10.1016/j.rse.2016.10.052

Krooks, A., Kaasalainen, S., Kankare, V., Joensuu, M., Raumonen, P., Kaasalainen, M., 2014. Tree structure vs. height from terrestrial laser scanning and quantitative structure

models. Silva Fennica. https://doi.org/10.14214/sf.1125
Kubiske, M.E., Abrams, M.D., 1991. Seasonal, diurnal and rehydration-induced variation of pressure-volume relationships in Pseudotsuga menziesii. Physiologia Plantarum. https://doi.org/10.1034/j.1399-3054.1991.830116.x
Liang, X., Kankare, V., Yu, X., Hyyppa, J., Holopainen, M., 2014. Automated Stem Curve Measurement Using Terrestrial Laser Scanning. IEEE Transactions on Geoscience and Remote Sensing. https://doi.org/10.1109/tgrs.2013.2253783
Lintunen, A., Paljakka, T., Salmon, Y., Dewar, R., Riikonen, A., Hölttä, T., 2020. The influence of soil temperature and water content on belowground hydraulic conductance and leaf gas exchange in mature trees of three boreal species. Plant Cell Environ. 43, 532–547. https://doi.org/10.1111/pce.13709
Martinez-Vilalta, J., Anderegg, W.R.L., Sapes, G., Sala, A., 2019. Greater focus on water pools may improve our ability to understand and anticipate drought-induced mortality in plants. New Phytol. 223, 22–32. https://doi.org/10.1111/nph.15644
McDowell, N.G., Allen, C.D., 2015. Darcy's law predicts widespread forest mortality under climate warming. Nature Climate Change. https://doi.org/10.1038/nclimate2641
Nevalainen, O., Hakala, T., Suomalainen, J., Mäkipää, R., Peltoniemi, M., Krooks, A., Kaasalainen, S., 2014. Fast and nondestructive method for leaf level chlorophyll estimation using hyperspectral LiDAR. Agricultural and Forest Meteorology. https://doi.org/10.1016/j.agrformet.2014.08.018
Nichol, J., Hang, L.K., Sing, W.M., 2006. Empirical correction of low Sun angle images in steeply sloping terrain: a slope-matching technique. International Journal of Remote Sensing. https://doi.org/10.1080/02781070500293414
Nobel, P.S., 1999. Physicochemical & Environmental Plant Physiology. Academic Press.
Olsson, K.A., Milthorpe, F.L., 1983. Diurnal and Spatial Variation in Leaf Water Potential and Leaf Conductance of Irrigated Peach Trees. Functional Plant Biology. https://doi.org/10.1071/pp9830291
Penuelas, J., Pinol, J., Ogaya, R., Filella, I., 1997. Estimation of plant water concentration by the reflectance Water Index WI (R900/R970). International Journal of Remote Sensing. https://doi.org/10.1080/014311697217396
Poorter, H., Niinemets, Ü., Poorter, L., Wright, I.J., Villar, R., 2009. Causes and consequences of variation in leaf mass per area (LMA): a meta-analysis. New Phytologist. https://doi.org/10.1111/j.1469-8137.2009.02830.x
Pyörälä, J., Kankare, V., Vastaranta, M., Rikala, J., Holopainen, M., Sipi, M., Hyyppä, J., Uusitalo, J., 2018. Comparison of terrestrial laser scanning and X-ray scanning in measuring Scots pine (Pinus sylvestris L.) branch structure. Scandinavian Journal of Forest Research. https://doi.org/10.1080/02827581.2017.1355409
Rallo, G., Minacapilli, M., Ciraolo, G., Provenzano, G., 2014. Detecting crop water status in mature olive groves using vegetation spectral measurements. Biosystems Engineering 128, 52–68. https://doi.org/10.1016/j.biosystemseng.2014.08.012
R. Core Team, 2015. An Introduction to R. Samurai Media Limited.
Santos, A.O., Kaye, O., 2009. Grapevine leaf water potential based upon near infrared spectroscopy. Scientia Agricola. https://doi.org/10.1590/s0103-90162009000300001
Scholander, P.F., Bradstreet, E.D., Hemmingsen, E.A., Hammel, H.T., 1965. Sap Pressure in

Vascular Plants: Negative hydrostatic pressure can be measured in plants. Science 148, 339–346. https://doi.org/10.1126/science.148.3668.339

Sevanto, S., Vesala, T., Peramaki, M., Nikinmaa, E., 2002. Time lags for xylem and stem diameter variations in a Scots pine tree. Plant, Cell and Environment. https://doi.org/10.1046/j.1365-3040.2002.00884.x

Syvertsen, J.P., Levy, Y., 1982. Diurnal Changes in Citrus Leaf Thickness, Leaf Water Potential and Leaf to Air Temperature Difference. Journal of Experimental Botany. https://doi.org/10.1093/jxb/33.4.783

Trenberth, K.E., 2011. Changes in precipitation with climate change. Climate Research. https://doi.org/10.3354/cr00953

Wagner, W., Ullrich, A., Ducic, V., Melzer, T., Studnicka, N., 2006. Gaussian decomposition and calibration of a novel small-footprint full-waveform digitising airborne laser scanner. ISPRS Journal of Photogrammetry and Remote Sensing. https://doi.org/10.1016/j.isprsjprs.2005.12.001

Wheeler, T., von Braun, J., 2013. Climate Change Impacts on Global Food Security. Science. https://doi.org/10.1126/science.1239402

Yrttimaa, T., Saarinen, N., Luoma, V., Tanhuanpää, T., Kankare, V., Liang, X., Hyyppä, J., Holopainen, M., Vastaranta, M., 2019. Detecting and characterizing downed dead wood using terrestrial laser scanning. ISPRS journal of photogrammetry and remote sensing 151, 76–90. https://doi.org/10.31219/osf.io/t2h8r